



# High Blocking Temperature of Magnetization and Giant Coercivity in the Azafullerene $Tb_2@C_{79}N$ with a Single-Electron Terbium–Terbium Bond

Georgios Velkos, Denis S. Krylov, Kyle Kirkpatrick, Lukas Spree, Vasilii Dubrovin, Bernd Büchner, Stanislav M. Avdoshenko, Valeriy Bezmelnitsyn, Sean Davis, Paul Faust, James Duchamp, Harry C. Dorn,\* and Alexey A. Popov\*

**Abstract:** The azafullerene  $Tb_2@C_{79}N$  is found to be a single-molecule magnet with a high 100-s blocking temperature of magnetization of 24 K and large coercivity. Tb magnetic moments with an easy-axis single-ion magnetic anisotropy are strongly coupled by the unpaired spin of the single-electron Tb–Tb bond. Relaxation of magnetization in  $Tb_2@C_{79}N$  below 15 K proceeds via quantum tunneling of magnetization with the characteristic time  $\tau_{QTM} = 16462 \pm 1230$  s. At higher temperature, relaxation follows the Orbach mechanism with a barrier of  $757 \pm 4$  K, corresponding to the excited states, in which one of the Tb spins is flipped.

The ongoing quest for lanthanide single-molecule magnets (SMMs) operating at ever higher temperatures resulted in impressive progress over the last decades,<sup>[1]</sup> culminating in the recent discovery of blocking of magnetization above liquid-nitrogen temperature in Dy-metalloenes.<sup>[2]</sup> On the next step from fundamental research to prospective applications, that is, as components of spintronic devices, the stability and processability of SMM materials has to be considered. Air-stability, thermal stability, and the ability to form thin molecular layers on different substrates are among the critical issues. Encapsulation of magnetic species within robust

molecular containers appears to be a practical route towards SMMs fulfilling the required stability criteria.

The chemical and thermal stability of fullerenes makes them perfectly suitable for this goal. They can encapsulate up to four metal atoms within their inner space (hence the term endohedral metallofullerenes, EMFs),<sup>[3]</sup> and a number of lanthanide EMFs exhibit SMM properties.<sup>[4]</sup> Besides, EMF-SMMs can form monolayers by sublimation or by self-assembly from solution, and such monolayers retain their SMM properties on metallic substrates.<sup>[5]</sup> Herein, we demonstrate that encapsulation of a  $Tb_2$  dimer within the azafullerene  $C_{79}N$  gives an excellent air-stable SMM.

Dimetallofullerenes  $Ln_2@C_{80-I_h}$  of early lanthanides ( $Ln = La-Nd$ ) were among the first synthesized EMF species.<sup>[6]</sup> In these molecules, metal atoms adopt a trivalent state, and the  $Ln_2$  dimer transfers six valence electrons to the carbon cage. At the same time,  $Ln_2@C_{80}$  molecules for heavier lanthanides (Gd and beyond) or Y could not be isolated, despite the high abundance of other EMFs with these metals. In 2008, it was found that a stable form of  $Ln_2@C_{80}$  species with heavy lanthanides is obtained if one carbon atom is substituted by nitrogen with the formation of azafullerenes,  $Ln_2@C_{79}N$  ( $Ln = Y, Gd, Tb$ ).<sup>[7]</sup>

The reason for the low stability of  $Ln_2@C_{80}$  molecules with heavy lanthanides is the low energy of the  $Ln-Ln$  bonding molecular orbital (MO) in the  $Ln_2$  dimers. When  $Ln_2$  is encapsulated in the  $C_{80}$  cage, only five electrons are transferred to the fullerene instead of six required to obtain stable closed-shell electronic structure of  $C_{80-I_h}$ .<sup>[8]</sup>  $Ln_2^{5+}@C_{80}^{5-}$  can be indeed stabilized by a single-electron reduction in the anionic form  $Ln_2^{5+}@C_{80}^{6-}$ ,<sup>[9]</sup> and the stable neutral derivative  $Ln_2@C_{80}(CH_2Ph)$  can then be obtained by a substitution reaction of  $Ln_2@C_{80}^-$  with benzyl bromide.<sup>[4g,j]</sup> Substitution of carbon by nitrogen is another way to add a “missing” electron to  $C_{80}^{5-}$ , as the closed-shell  $C_{79}N^{5-}$  azafullerene cage is isoelectronic to  $C_{80}^{6-}$  (Figure 1).<sup>[7]</sup>


A distinctive feature of  $Ln_2@C_{79}N$  and  $Ln_2@C_{80}(CH_2Ph)$  molecules is the single-electron  $Ln-Ln$  bond (whose presence does not affect the air-stability). As follows from DFT calculations and EPR spectroscopic studies, the  $Ln-Ln$  bonding MO has an spd character (e.g., large contribution of 5s atomic orbitals is evidenced by the large hyperfine coupling constant in Y analogues).<sup>[4g,7b]</sup> The electron delocalized between metal atoms acts as a mediator between two localized Ln spins and strongly couples them together.<sup>[10]</sup> EPR spectroscopy revealed that Gd and electron spins in


[\*] G. Velkos, D. S. Krylov, L. Spree, V. Dubrovin, Prof. Dr. B. Büchner, Dr. S. M. Avdoshenko, Dr. A. A. Popov  
 Leibniz Institute for Solid State and Materials Research  
 Helmholtzstrasse 20, 01069 Dresden (Germany)  
 E-mail: a.popov@ifw-dresden.de

D. S. Krylov  
 Center for Quantum Nanoscience, Institute for Basic Science (IBS)  
 Seoul (Republic of Korea)

K. Kirkpatrick, P. Faust, Prof. Dr. J. Duchamp, Prof. Dr. H. C. Dorn  
 Department of Chemistry  
 Virginia Polytechnic Institute and State University  
 Blacksburg, Virginia 24061 (USA)  
 E-mail: hdorn@vt.edu

Dr. V. Bezmelnitsyn, S. Davis  
 Luna nanoWorks, a Division of Luna Innovation Inc.  
 521 Bridge St, Danville, Virginia (USA)

 Supporting information and the ORCID identification number(s) for the author(s) of this article can be found under:  
<https://doi.org/10.1002/anie.201900943>.

 © 2019 The Authors. Published by Wiley-VCH Verlag GmbH & Co. KGaA. This is an open access article under the terms of the Creative Commons Attribution Non-Commercial License, which permits use, distribution and reproduction in any medium, provided the original work is properly cited, and is not used for commercial purposes.

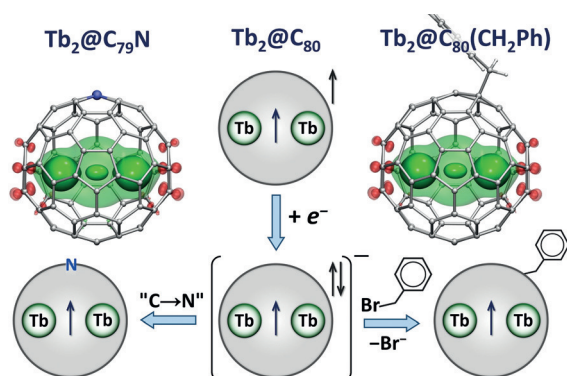


**Figure 1.** Schematic depiction of  $\text{Tb}_2@C_{80}$  with a single-electron Tb–Tb bond and an unpaired spin on the fullerene cage, which can be stabilized by addition of an electron, substitution of one carbon atom by nitrogen to yield azafullerene  $\text{Tb}_2@C_{79}\text{N}$ , or by functionalization with a radical group, as realized in  $\text{Tb}_2@C_{80}(\text{CH}_2\text{Ph})$ . Also shown are spin density distributions in  $\text{Ln}_2@C_{79}\text{N}$  and  $\text{Ln}_2@C_{80}(\text{CH}_2\text{Ph})$  (low isovalue for semitransparent isosurface, and high isovalue for solid isosurface). Three regions with high spin density correspond to 4f-electrons of two Ln atoms and to the unpaired electron residing on the Ln–Ln bonding orbital.

$\text{Gd}_2@C_{79}\text{N}$  are coupled ferromagnetically giving the total spin of  $S=15/2$ ,<sup>[7a,11]</sup> and magnetometry studies showed that the Gd-electron coupling constant in  $\text{Gd}_2@C_{79}\text{N}$  is as large as  $K^{\text{eff}}=170\pm 10\text{ cm}^{-1}$  (spin Hamiltonian  $-2K^{\text{eff}}\hat{S}(\hat{S}_{\text{Gd}-1}+\hat{S}_{\text{Gd}-2})$ ).<sup>[11a,12]</sup> Similar characteristics were also found in  $\text{Gd}_2@C_{80}(\text{CH}_2\text{Ph})$ <sup>[4j]</sup> as both molecules have three-center spin system [ $\text{Gd}^{3+}-e-\text{Gd}^{3+}$ ]. The single-electron bond can thus be considered as an ultimate realization of the radical-bridge concept.<sup>[13]</sup> Exploiting this concept gave a number of poly-nuclear lanthanide compounds with enhanced lanthanide-radical exchange coupling and interesting SMM properties.<sup>[14]</sup> For anisotropic lanthanides, the [ $\text{Ln}^{3+}-e-\text{Ln}^{3+}$ ] system with strong coupling may result in outstanding SMM behavior. A large relaxation barrier was predicted for  $\text{Dy}_2@C_{79}\text{N}$ .<sup>[10b]</sup>  $\text{Dy}_2@C_{80}(\text{CH}_2\text{Ph})$  was found to be a SMM with a high 100-s blocking temperature of 18 K.<sup>[4g]</sup> Even better SMM performance was found in  $\text{Tb}_2@C_{80}(\text{CH}_2\text{Ph})$ .<sup>[4j]</sup> Herein, we report the first magnetic study of a dimetallo-azafullerene with an anisotropic lanthanide,  $\text{Tb}_2@C_{79}\text{N}$ , and demonstrate that the [ $\text{Tb}^{3+}-e-\text{Tb}^{3+}$ ] spin system protected inside the  $C_{79}\text{N}$  cage yields exceptional SMM properties.

$\text{Tb}_2@C_{79}\text{N}$  was previously prepared via a Krätschmer-Huffman electric-arc process with a  $\text{He}/\text{N}_2$  (280/20 torr) atmosphere by vaporizing packed  $\text{Tb}_4\text{O}_7$  graphite rods,<sup>[7b]</sup> but the sample for the current study was synthesized by a 3-phase electric arc discharge evaporation of graphite rods with  $\text{Tb}_4\text{O}_7$  powder injection into the 3-phase electric arc zone in only a  $\text{N}_2$  atmosphere.<sup>[15]</sup> This leads to a significant change in the EMF distribution with a higher concentration of nitrogen containing metallofullerene species after a usual amino silica separation step (Figure S1–S3 in the Supporting Information).<sup>[16]</sup> In a final step, recycling HPLC was used to obtain pure  $\text{Tb}_2@C_{79}\text{N}$  (Figure S4–S5). HPLC separation also showed the presence of a new EMF in the  $\text{Tb}_2@C_{79}\text{N}$  fraction with the composition  $\text{Tb}_2\text{C}_{80}\text{N}_2$  (Figure S3 and S5). The most likely structure of this compound is  $\text{Tb}_2\text{CN}@C_{79}\text{N}$  with the

charge distribution  $(\text{Tb}^{3+})_2(\text{CN})^-@(\text{C}_{79}\text{N})^{5-}$ . This di-metallic cyanide-clusterfullerene complements a series of  $\text{TbCN}@C_{2n}$  EMFs discovered by Yang et al.<sup>[14a,17]</sup> Unfortunately, the low yield of  $\text{Tb}_2\text{CN}@C_{79}\text{N}$  precludes its detailed characterization at this time.

The molecular structure of  $\text{Tb}_2@C_{79}\text{N}$  was elucidated earlier by single-crystal X-ray diffraction proving that the fullerene cage is based on the  $C_{80}-I_h$  isomer with one carbon atom substituted by nitrogen.<sup>[7b]</sup> The exact position of the nitrogen atom cannot be determined from diffraction data. DFT calculations<sup>[18]</sup> show that in the most stable isomers, the nitrogen substitutes carbon on the pentagon/hexagon/hexagon vertex. The  $\text{Tb}_2$  dimer has several virtually isoenergetic orientations inside the  $C_{79}\text{N}$  cage, including the one shown in Figure 1 (see Table S1 for all stable conformers).

Magnetic properties of the  $\text{Tb}_2@C_{79}\text{N}$  powder sample were studied by SQUID magnetometry. Figure 2a shows the magnetic susceptibility  $\chi$  of the zero-field cooled sample measured during in-field heating to the one measured during in-field cooling of the same sample. The blocking temperature

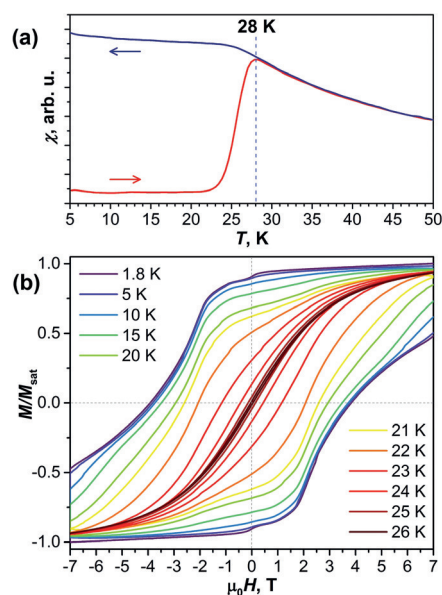


**Figure 2.** a) Determination of the blocking temperature of magnetization,  $T_B$ , for  $\text{Tb}_2@C_{79}\text{N}$  ( $\mu_0H=0.2\text{ T}$ , temperature sweep rate  $5\text{ K min}^{-1}$ ); b) Magnetic hysteresis of  $\text{Tb}_2@C_{79}\text{N}$  measured between 1.8 and 26 K (sweep rate  $2.9\text{ mT s}^{-1}$ ).

of magnetization  $T_B$ , determined from these measurements, is 28 K (temperature sweep rate of  $5\text{ K min}^{-1}$ ). This is only 1 K short of 29 K determined for  $\text{Tb}_2@C_{80}(\text{CH}_2\text{Ph})$ .<sup>[4j]</sup> Thus, the [ $\text{Tb}^{3+}-e-\text{Tb}^{3+}$ ] spin system with two local Tb spins and delocalized unpaired electron offers the highest  $T_B$  among dinuclear and radical-bridged SMMs. The only dinuclear SMM with similarly high blocking temperature is a Tb complex with a  $\text{N}_2^{3-}$  radical bridge.<sup>[14a]</sup> In agreement with its high  $T_B$ ,  $\text{Tb}_2@C_{79}\text{N}$  exhibits magnetic hysteresis up to 27 K when measured with a moderate sweep rate of  $2.9\text{ mT s}^{-1}$ . The hysteresis is very broad with a coercive field of 3.8 T between 1.8 and 10 K.

Zero-field relaxation times of magnetization  $\tau_m$  below 24 K were determined by stretched exponential fitting of magnetization decay curves recorded after the fast sweep of magnetic field from 7 T to 0 T (Table S2, Figure S6). Between 31 and 39 K,  $\tau_m$  values were determined from  $\chi'/\chi''$  susceptibilities and Cole–Cole plots measured by AC magnetometry (Figure 3 and Figure S7, Table S3).

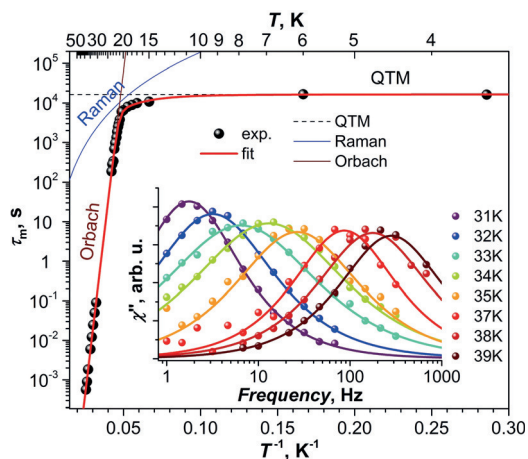


**Figure 3.** Relaxation times of magnetization of  $\text{Tb}_2@C_{79}\text{N}$  measured in zero field (dots); lines are results of the fit with Equation (1) and contributions of different relaxation mechanisms. The inset shows the out-of-phase magnetic susceptibility  $\chi''$  measured at different temperatures (dots) and fits with generalized Debye model (lines).

The temperature dependence of  $\tau_m$  of  $\text{Tb}_2@C_{79}\text{N}$  can be described by a combination of the temperature-independent quantum tunneling of magnetization (QTM), the Raman mechanism with power dependence on temperature, and the Orbach mechanism with exponential temperature dependence [Eq. (1)]:

$$\tau_m^{-1}(T) = \tau_{\text{QTM}}^{-1} + CT^n + \tau_0^{-1}\exp(-U^{\text{eff}}/T) \quad (1)$$

Fitting the  $\tau_m$  values with Equation (1) shows that below 15 K the relaxation proceeds via the QTM with  $\tau_{\text{QTM}}$  of  $16462 \pm 1230$  s. Orbach mechanism with a barrier of  $U^{\text{eff}} = 757 \pm 4$  K and an attempt time  $\tau_0 = (2.4 \pm 0.4) \times 10^{-12}$  s dominates at  $T > 22$  K (linear regime in Arrhenius coordinates, Figure 3). In the transition region between 15 and 22 K, a contribution of the Raman mechanism with  $n = 3.9 \pm 1.0$  is also visible. From the  $\tau_m - T$  dependence, the 100-s blocking temperature is determined as  $T_{\text{B}100} = 24.1$  K.

The following spin Hamiltonian is used for  $\text{Tb}_2@C_{79}\text{N}$  [Eq. (2)]:

$$\hat{H}_{\text{spin}} = \hat{H}_{\text{LF}_1} + \hat{H}_{\text{LF}_2} - 2K^{\text{eff}}\hat{s}(\hat{J}_1 + \hat{J}_2) + \hat{H}_{\text{ZEE}} \quad (2)$$

where  $\hat{H}_{\text{LF}_i}$  is the single-ion ligand-field Hamiltonian for the  $i$ -th terbium site,  $K^{\text{eff}}$  is an isotropic exchange coupling constant between the localized terbium moment  $\hat{J}_i$  and electron spin  $\hat{s}$ , and  $\hat{H}_{\text{ZEE}}$  is the Zeeman term. In essence, the molecule is treated as a three-center spin system,<sup>[10a,b,12,14a,19]</sup> where direct

$\text{Tb}\cdots\text{Tb}$  exchange is neglected (hence the effective coupling constant  $K^{\text{eff}}$  in the exchange term<sup>[4j,12]</sup>). Terbium moments  $\hat{J}_i$  are treated in the  $|J, m_J\rangle$  basis sets of each ion ( ${}^7F_6$  multiplet). Powder averaging is used as implemented in the PHI code.<sup>[20]</sup>

To obtain the ligand-field parameters for Tb ions, we performed ab initio calculations at the CASSCF(8,7)/SO-RASSI<sup>[21]</sup> level for  $\text{TbY}@C_{79}\text{N}^-$ . Calculations for the non-charged  $\text{TbY}@C_{79}\text{N}$  molecule would require inclusion of the unpaired valence electron and its MO into the active space, which makes calculations less tractable. Besides, the ligand field parameters would then lose their clear physical meaning. Ab initio calculations showed that in  $\text{TbY}@C_{79}\text{N}^-$ , the  $\text{Tb}^{3+}$  ion has easy-axis magnetic anisotropy with the quantization axis aligned along the Tb–Tb bond, but tilted from it by approximately  $7^\circ$ . The tilting angle is varying slightly depending on the orientation of the  $\text{Tb}_2$  dimer inside  $C_{79}\text{N}$  (Figure S8). Although  $\text{Tb}^{3+}$  is not a Kramers ion, the strong axiality results in the grouping of the ligand-field states into pseudo-doublets (pKD) with a small splitting within each pKD. In  $|J, m_J\rangle$  basis, the low-energy pKD states have almost pure  $m_J$  composition (Table S4–S8). The contribution of  $|m_J| = 6$  in the ground pKD is 99.9%, the second pKD at  $265\text{ cm}^{-1}$  is  $|m_J| = 5$  (99.6%), and the third pKD at  $511\text{ cm}^{-1}$  is  $|m_J| = 4$  (98.9%). The overall ligand-field splitting is  $1014\text{ cm}^{-1}$ .

Figure 4a shows simulated  $\chi T$  curves for different values of  $K^{\text{eff}}$  to the experimental curve measured in a field of 1 T.

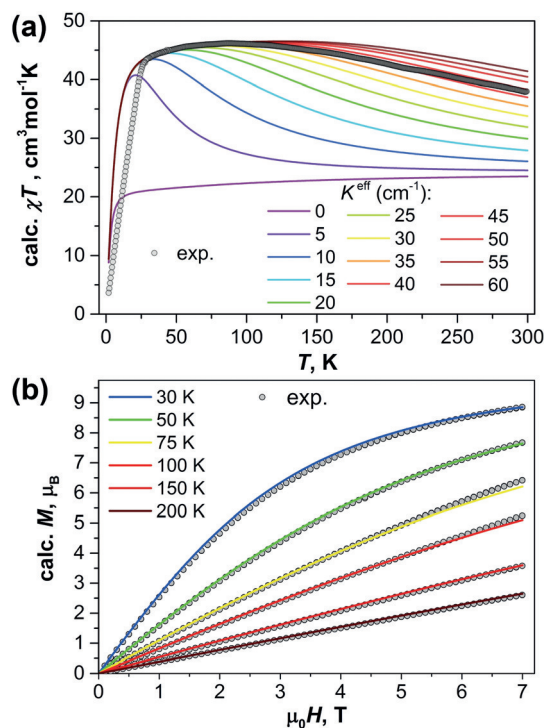


**Figure 4.** a) Experimental  $\chi T$  curve for  $\text{Tb}_2@C_{79}\text{N}$  measured in the field of 1 T and the simulations with different values of  $K^{\text{eff}}$  (lines); note that below  $T_B$ , the experimental curve does not represent the thermodynamic behavior and cannot be reproduced by simulations. b) Experimental magnetization curves of  $\text{Tb}_2@C_{79}\text{N}$  measured at different temperatures above  $T_B$  and the simulations with  $K^{\text{eff}} = 45\text{ cm}^{-1}$ . Experimental data are in arbitrary units scaled to match simulated curves.

Reasonable agreement is achieved at  $K^{\text{eff}}$  values of 40–45  $\text{cm}^{-1}$ . Magnetization curves simulated for the  $K^{\text{eff}}$  constant of 45  $\text{cm}^{-1}$  agree well with the experimental data (Figure 4b). Note that the sign of  $K^{\text{eff}}$  is difficult to determine because magnetization data does not change much when the sign of  $K^{\text{eff}}$  is reversed. However, magnetization and EPR data on the Gd analogue,  $\text{Gd}_2@C_{79}\text{N}$ , clearly point to the positive value of  $K^{\text{eff}}$  in that molecule.<sup>[7a,11,12]</sup> We thus suggest that the positive sign of  $K^{\text{eff}}$  is more likely for  $\text{Tb}_2@C_{79}\text{N}$  as well.

It is instructive to analyze the spectrum of the Hamiltonian (2) shown in Figure 5 (and Table S9) for the understanding of the relaxation behavior of  $\text{Tb}_2@C_{79}\text{N}$ . As a Kramers system,  $[\text{Tb}^{3+}-e-\text{Tb}^{3+}]$  has a rigorous two-fold degeneracy

of the spin states in zero magnetic field. In the ground state doublet, all three spins are aligned along the Tb–Tb axis (Figure 5a,b) giving a total magnetic moment of 18.9  $\mu_B$ . This giant-spin state can be described as a pseudospin  $S = 1/2$  with the  $g$ -tensor (0, 0, 37.789). Negligible transverse ( $x,y$ ) components of the  $g$ -tensor and the large total spin result in the low efficiency of the QTM, in which the total spin flips as a whole (hence the long QTM relaxation time of ca. 5 hours).

The lowest energy excited states at 251 and 310  $\text{cm}^{-1}$  correspond to the ligand-field excitation in one of the Tb ions to the second pKD. Further states with ligand-field excitations to the third pKD, or when both Tb centers are excited to the second pKD, are found at 494, 541, and 609  $\text{cm}^{-1}$ . All these states are characterized by negligible  $g_{x,y}$  components and  $g_z$  values of 34.7–34.8 (states at 251 and 310  $\text{cm}^{-1}$ ) and 31.7–31.8 (states at 494, 541, and 609  $\text{cm}^{-1}$ ). The transition probabilities within these doublets are very low (below  $10^{-7} \mu_B^2$ ).

More important for the relaxation of magnetization in  $\text{Tb}_2@C_{79}\text{N}$  are exchange-excited states, in which one of the Tb spins is flipped. If two symmetry-equivalent and collinear Tb spins are ferromagnetically coupled to the spin 1/2, the exchange-excited states with flipping of one Tb spin would form a quartet. But if Tb ions are not magnetically equivalent, or if their spins are tilted from the Tb–Tb axis, then the quartet is split into two doublets. Our simulations with Equation (2) and  $K^{\text{eff}}$  of 45  $\text{cm}^{-1}$  show that the splitting increases very quickly with increasing tilting angle  $\alpha$  (Figure 5c). Furthermore, when one Tb spin is reversed, both Tb spins cancel each other in the  $z$  direction, but tilting leads to the emergence of  $y$ -component (if tilting is defined as a rotation around the  $x$ -axis). The unpaired electron spin then orients itself along the  $y$ -axis either parallel or antiparallel to the projection of Tb moments as illustrated schematically in Figure 5b,c. The two states thus have different  $g_y$  factors (Figure 5c;  $g_x$  and  $g_z$  are virtually zero). In particular, for  $\text{Tb}_2@C_{79}\text{N}$  with a tilting angle of 7.2° and isotropic  $K^{\text{eff}} = 45 \text{ cm}^{-1}$ , the lowest-energy exchange-excited states are found at 410  $\text{cm}^{-1}$  ( $g_y = 11.61$ ) and 505  $\text{cm}^{-1}$  ( $g_y = 0.79$ ). Note that these energies deviate significantly from  $2JK^{\text{eff}} = 540 \text{ cm}^{-1}$ .

With negligible  $g_z$  components, exchange excited states should be very efficient for the spin reversal. When ligand-field excited and exchange-excited states have similar energies, transition probabilities between them can become sufficiently high (Figure 5b), and this may be a relevant relaxation pathway for the Orbach relaxation mechanism. Alternatively, the system can be excited to the exchange states directly from the ground state. A simple spin Hamiltonian employed in this work gives a very low transition probability for such a process. However, more refined treatment proposed by Chibotaru et al. for the radical-bridged di-Tb complex showed that exchange excitations may have a rather high transition probability.<sup>[19]</sup> In either case, we can conclude that the Orbach relaxation with  $U^{\text{eff}}$  of 757 K (526  $\text{cm}^{-1}$ ) proceeds via flipping of one of the Tb moments.

It is interesting to compare SMM properties of  $\text{Tb}_2@C_{79}\text{N}$  and  $\text{Tb}_2@C_{80}(\text{CH}_2\text{Ph})$ , as these molecules have identical spin system encapsulated in the same fullerene cage but with different “defects” (one nitrogen atom in the azafullerene

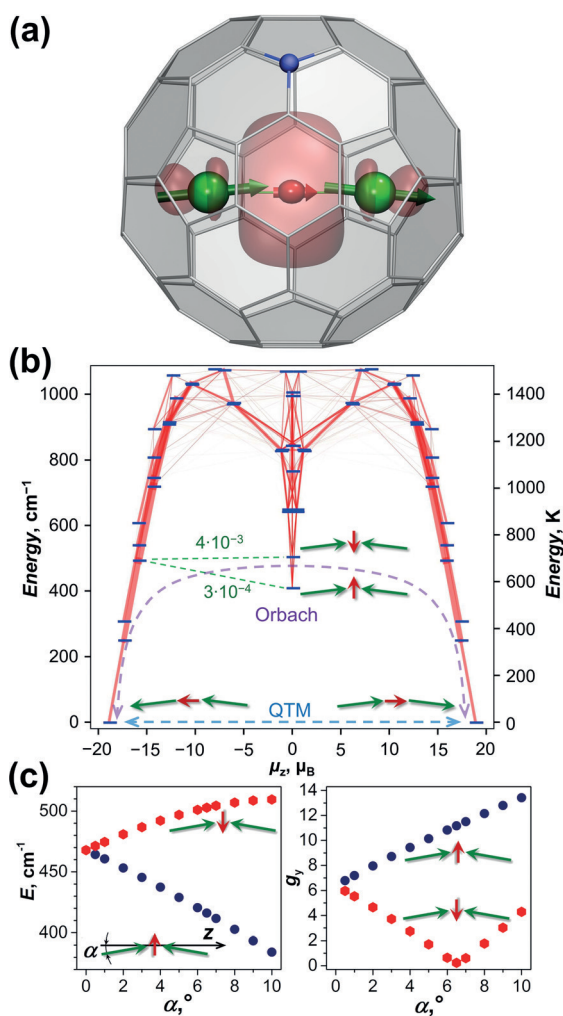


**Figure 5.** a) Alignment of individual spins in  $\text{Tb}_2@C_{79}\text{N}$  in the ground state (quantization axes of Tb ions are shown as green arrows, the red arrow represents the unpaired electron spin, whereas red isosurfaces represent the valence spin density distribution). b) Low-energy part of the spectrum of the Hamiltonian (2) with  $K^{\text{eff}} = 45 \text{ cm}^{-1}$ ; dashed arrows denote QTM and Orbach relaxation mechanisms, numbers are transition probabilities (in  $\mu_B^2$ ), thickness of the red lines between the levels scales with transition probability. c) Dependence of the energy (left) and  $g_y$  component (right) of the lowest-energy exchange-excited states as a function of the tilting angle  $\alpha$ . Green and red arrows schematically show alignment of the magnetic moments of Tb (green) and the unpaired electron (red).

versus one C-sp<sup>3</sup> atom in the benzyl adduct). It appears that Tb<sub>2</sub>@C<sub>80</sub>(CH<sub>2</sub>Ph) is the slightly stronger SMM with T<sub>B</sub> and T<sub>B100</sub> values of 29 and 25 K, respectively.<sup>[4j]</sup> It also shows broader hysteresis, longer QTM relaxation time of 18 h and a higher thermal relaxation barrier of U<sup>eff</sup> = 799 K. Thus, despite the overall similarity of the two SMMs, we can conclude that the fullerene cage is not just an inert container but has a certain influence on the SMM behavior. Importantly, magnetic moments of Tb ions in Tb<sub>2</sub>@C<sub>80</sub>(CH<sub>2</sub>Ph) are not tilted from the Tb...Tb axis. The role of the substitutional "defect" in C<sub>80</sub> cage is clearly seen in the electrostatic potential (ESP) distribution (Table S10). In C<sub>80</sub><sup>6-</sup> the ESP is virtually isotropic, which is consistent with the I<sub>h</sub> symmetry of the fullerene cage. Substitution of one carbon by nitrogen imposes a strong asymmetry of the ESP. This strong variation of the ESP may explain why metal atoms in Tb<sub>2</sub>@C<sub>79</sub>N tend to avoid positions near nitrogen atom. Presumably, tilting of the quantization axes of Tb ions in Tb<sub>2</sub>@C<sub>79</sub>N from the Tb...Tb axis is also caused by this strong anisotropy of the ESP. C-sp<sup>3</sup> atom in C<sub>80</sub>(CH<sub>2</sub>Ph)<sup>5-</sup> also imposes similar asymmetry in ESP, but it is less pronounced than in the azafullerene. Therefore, a modification of the fullerene host, for example, by chemical derivatization, may be used to further tune magnetic properties of endohedral lanthanide dimers.

To conclude, we have demonstrated that Tb<sub>2</sub>@C<sub>79</sub>N is a strong single-molecule magnet with a 100-s blocking temperature of magnetization of 24 K and a large Tb-electron exchange coupling constant of 40–45 cm<sup>-1</sup>. Together with the recently studied Tb<sub>2</sub>@C<sub>80</sub>(CH<sub>2</sub>Ph), this system shows that encapsulation of the Tb<sub>2</sub> dimer with a single-electron Tb–Tb bond inside fullerene cages is a viable route to air-stable single-molecule magnets with high blocking temperatures and large coercive fields. Furthermore, unlike Tb<sub>2</sub>@C<sub>80</sub>(CH<sub>2</sub>Ph), Tb<sub>2</sub>@C<sub>79</sub>N has no exohedral substituents on the fullerene cage, which leads to a higher thermal stability and allows growth of thin molecular films via sublimation.

## Acknowledgements

We acknowledge funding from the European Union's Horizon 2020 research and innovation programme, European Research Council (grant agreement No 648295 to A.A.P.), and Marie Skłodowska-Curie action (grant agreement No. 748635 to S.M.A.), and the Deutsche Forschungsgemeinschaft (grants PO 1602/4-1 and 1602/5-1 to A.A.P.). K.K. acknowledges financial support from a Luther & Alice Hamlett Scholarship. Computational resources were provided by the Center for High Performance Computing at the TU Dresden. We appreciate the help from Dr. Anja U. B. Wolter and Sebastian Gaß in magnetic measurements and technical support with computational resources in IFW Dresden by Ulrike Nitzsche.

## Conflict of interest

The authors declare no conflict of interest.

**Keywords:** endohedral fullerenes · exchange coupling · metal–metal bonds · single-molecule magnets · terbium

**How to cite:** *Angew. Chem. Int. Ed.* **2019**, *58*, 5891–5896  
*Angew. Chem.* **2019**, *131*, 5951–5956

- [1] a) J. Luzon, R. Sessoli, *Dalton Trans.* **2012**, *41*, 13556–13567; b) L. Sorace, C. Benelli, D. Gatteschi, *Chem. Soc. Rev.* **2011**, *40*, 3092–3104; c) J.-L. Liu, Y.-C. Chen, M.-L. Tong, *Chem. Soc. Rev.* **2018**, *47*, 2431–2453; d) S. T. Liddle, J. van Slageren, *Chem. Soc. Rev.* **2015**, *44*, 6655–6669; e) J. Dreiser, *J. Phys. Condens. Matter* **2015**, *27*, 183203.
- [2] a) C. A. P. Goodwin, F. Ortu, D. Reta, N. F. Chilton, D. P. Mills, *Nature* **2017**, *548*, 439–442; b) F.-S. Guo, B. M. Day, Y.-C. Chen, M.-L. Tong, A. Mansikkamäki, R. A. Layfield, *Angew. Chem. Int. Ed.* **2017**, *56*, 11445–11449; *Angew. Chem.* **2017**, *129*, 11603–11607; c) F.-S. Guo, B. M. Day, Y.-C. Chen, M.-L. Tong, A. Mansikkamäki, R. A. Layfield, *Science* **2018**, *362*, 1400–1403; d) K. R. McClain, C. A. Gould, K. Chakarawet, S. Teat, T. J. Groshens, J. R. Long, B. G. Harvey, *Chem. Sci.* **2018**, *9*, 8492–8503.
- [3] a) A. A. Popov, S. Yang, L. Dunsch, *Chem. Rev.* **2013**, *113*, 5989–6113; b) S. Yang, T. Wei, F. Jin, *Chem. Soc. Rev.* **2017**, *46*, 5005–5058.
- [4] a) F. Liu, C.-L. Gao, Q. Deng, X. Zhu, A. Kostanyan, R. Westerström, S. Wang, Y.-Z. Tan, J. Tao, S.-Y. Xie, A. A. Popov, T. Greber, S. Yang, *J. Am. Chem. Soc.* **2016**, *138*, 14764–14771; b) K. Junghans, C. Schlesier, A. Kostanyan, N. A. Samoylova, Q. Deng, M. Rosenkranz, S. Schiemenz, R. Westerström, T. Greber, B. Büchner, A. A. Popov, *Angew. Chem. Int. Ed.* **2015**, *54*, 13411–13415; *Angew. Chem.* **2015**, *127*, 13609–13613; c) R. Westerström, J. Dreiser, C. Piamonteze, M. Muntwiler, S. Weyeneth, K. Krämer, S.-X. Liu, S. Decurtins, A. Popov, S. Yang, L. Dunsch, T. Greber, *Phys. Rev. B* **2014**, *89*, 060406; d) R. Westerström, J. Dreiser, C. Piamonteze, M. Muntwiler, S. Weyeneth, H. Brune, S. Rusponi, F. Nolting, A. Popov, S. Yang, L. Dunsch, T. Greber, *J. Am. Chem. Soc.* **2012**, *134*, 9840–9843; e) D. Krylov, F. Liu, A. Brandenburg, L. Spree, V. Bon, S. Kaskel, A. Wolter, B. Büchner, S. Avdoshenko, A. A. Popov, *Phys. Chem. Chem. Phys.* **2018**, *20*, 11656–11672; f) D. S. Krylov, F. Liu, S. M. Avdoshenko, L. Spree, B. Weise, A. Waske, A. U. B. Wolter, B. Büchner, A. A. Popov, *Chem. Commun.* **2017**, *53*, 7901–7904; g) F. Liu, D. S. Krylov, L. Spree, S. M. Avdoshenko, N. A. Samoylova, M. Rosenkranz, A. Kostanyan, T. Greber, A. U. B. Wolter, B. Büchner, A. A. Popov, *Nat. Commun.* **2017**, *8*, 16098; h) C.-H. Chen, D. S. Krylov, S. M. Avdoshenko, F. Liu, L. Spree, R. Yadav, A. Alvertis, L. Hozoi, K. Nenkov, A. Kostanyan, T. Greber, A. U. B. Wolter, A. A. Popov, *Chem. Sci.* **2017**, *8*, 6451–6465; i) J. Dreiser, R. Westerström, Y. Zhang, A. A. Popov, L. Dunsch, K. Krämer, S.-X. Liu, S. Decurtins, T. Greber, *Chem. Eur. J.* **2014**, *20*, 13536–13540; j) F. Liu, G. Velkos, D. S. Krylov, L. Spree, M. Zalibera, R. Ray, N. A. Samoylova, C.-H. Chen, M. Rosenkranz, S. Schiemenz, F. Ziegls, K. Nenkov, A. Kostanyan, T. Greber, A. U. B. Wolter, M. Richter, B. Büchner, S. M. Avdoshenko, A. A. Popov, *Nat. Commun.* **2019**, *10*, 571; k) C. Schlesier, L. Spree, A. Kostanyan, R. Westerström, A. Brandenburg, A. U. B. Wolter, S. Yang, T. Greber, A. A. Popov, *Chem. Commun.* **2018**, *54*, 9730–9733; l) A. Brandenburg, D. S. Krylov, A. Beger, A. U. B. Wolter, B. Büchner, A. A. Popov, *Chem. Commun.* **2018**, *54*, 10683–10686.
- [5] a) C. H. Chen, D. S. Krylov, S. M. Avdoshenko, F. Liu, L. Spree, R. Westerström, C. Bulbucan, M. Studniarek, J. Dreiser, A. U. B. Wolter, B. Büchner, A. A. Popov, *Nanoscale* **2018**, *10*, 11287–11292; b) R. Westerström, A.-C. Uldry, R. Stania, J. Dreiser, C. Piamonteze, M. Muntwiler, F. Matsui, S. Rusponi, H. Brune, S. Yang, A. Popov, B. Büchner, B. Delley, T. Greber, *Phys. Rev. Lett.* **2015**, *114*, 087201.

- [6] a) T. Suzuki, Y. Maruyama, T. Kato, K. Kikuchi, Y. Nakao, Y. Achiba, K. Kobayashi, S. Nagase, *Angew. Chem. Int. Ed. Engl.* **1995**, *34*, 1094–1096; *Angew. Chem.* **1995**, *107*, 1228–1230; b) J. Q. Ding, S. H. Yang, *J. Am. Chem. Soc.* **1996**, *118*, 11254–11257; c) J. Ding, S. Yang, *Angew. Chem. Int. Ed. Engl.* **1996**, *35*, 2234–2235; *Angew. Chem.* **1996**, *108*, 2369–2371.
- [7] a) W. Fu, J. Zhang, T. Fuhrer, H. Champion, K. Furukawa, T. Kato, J. E. Mahaney, B. G. Burke, K. A. Williams, K. Walker, C. Dixon, J. Ge, C. Shu, K. Harich, H. C. Dorn, *J. Am. Chem. Soc.* **2011**, *133*, 9741–9750; b) T. Zuo, L. Xu, C. M. Beavers, M. M. Olmstead, W. Fu, T. D. Crawford, A. L. Balch, H. C. Dorn, *J. Am. Chem. Soc.* **2008**, *130*, 12992–12997.
- [8] Z. Wang, R. Kitaura, H. Shinohara, *J. Phys. Chem. C* **2014**, *118*, 13953–13958.
- [9] A. Velloth, Y. Imamura, T. Kodama, M. Hada, *J. Phys. Chem. C* **2017**, *121*, 18169–18177.
- [10] a) F. Cimpoesu, B. Frecus, C. I. Oprea, H. Ramanantoanina, W. Urland, C. Daul, *Mol. Phys.* **2015**, *113*, 1712–1727; b) G. Rajaraman, M. K. Singh, N. Yadav, *Chem. Commun.* **2015**, *51*, 17732–17735; c) A. Mansikkamäki, A. A. Popov, Q. Deng, N. Iwahara, L. F. Chibotaru, *J. Chem. Phys.* **2017**, *147*, 124305.
- [11] a) Z. Hu, B.-W. Dong, Z. Liu, J.-J. Liu, J. Su, C. Yu, J. Xiong, D.-E. Shi, Y. Wang, B.-W. Wang, A. Ardavan, Z. Shi, S.-D. Jiang, S. Gao, *J. Am. Chem. Soc.* **2018**, *140*, 1123–1130; b) X. Wang, J. E. McKay, B. Lama, J. van Tol, T. Li, K. Kirkpatrick, Z. Gan, S. Hill, J. R. Long, H. C. Dorn, *Chem. Commun.* **2018**, *54*, 2425–2428.
- [12] G. Velkos, D. S. Krylov, K. Kirkpatrick, X. Liu, L. Spree, A. U. B. Wolter, B. Buchner, H. C. Dorn, A. A. Popov, *Chem. Commun.* **2018**, *54*, 2902–2905.
- [13] S. Demir, I.-R. Jeon, J. R. Long, T. D. Harris, *Coord. Chem. Rev.* **2015**, *289–290*, 149–176.
- [14] a) S. Demir, M. I. Gonzalez, L. E. Darago, W. J. Evans, J. R. Long, *Nat. Commun.* **2017**, *8*, 2144; b) K. R. Meihaus, J. F. Corbey, M. Fang, J. W. Ziller, J. R. Long, W. J. Evans, *Inorg. Chem.* **2014**, *53*, 3099–3107; c) J. D. Rinehart, M. Fang, W. J. Evans, J. R. Long, *Nat. Chem.* **2011**, *3*, 538–542; d) J. D. Rinehart, M. Fang, W. J. Evans, J. R. Long, *J. Am. Chem. Soc.* **2011**, *133*, 14236–14239.
- [15] V. Bezmelnitsyn, S. Davis, Z. Zhou, *Fullerenes Nanotubes Carbon Nanostruct.* **2015**, *23*, 612–617.
- [16] S. Stevenson, K. Harich, H. Yu, R. R. Stephen, D. Heaps, C. Coumbe, J. P. Phillips, *J. Am. Chem. Soc.* **2006**, *128*, 8829–8835.
- [17] a) F. Liu, S. Wang, J. Guan, T. Wei, M. Zeng, S. Yang, *Inorg. Chem.* **2014**, *53*, 5201–5205; b) F. Liu, S. Wang, C.-L. Gao, Q. Deng, X. Zhu, A. Kostanyan, R. Westerström, F. Jin, S.-Y. Xie, A. A. Popov, T. Greber, S. Yang, *Angew. Chem. Int. Ed.* **2017**, *56*, 1830–1834; *Angew. Chem.* **2017**, *129*, 1856–1860.
- [18] J. Hafner, *J. Comput. Chem.* **2008**, *29*, 2044–2078.
- [19] V. Vieru, N. Iwahara, L. Ungur, L. F. Chibotaru, *Sci. Rep.* **2016**, *6*, 24046.
- [20] N. F. Chilton, R. P. Anderson, L. D. Turner, A. Soncini, K. S. Murray, *J. Comput. Chem.* **2013**, *34*, 1164–1175.
- [21] a) F. Aquilante, J. Autschbach, R. K. Carlson, L. F. Chibotaru, M. G. Delcey, L. De Vico, I. Fdez. Galván, N. Ferré, L. M. Frutos, L. Gagliardi, M. Garavelli, A. Giussani, C. E. Hoyer, G. Li Manni, H. Lischka, D. Ma, P. Å. Malmqvist, T. Müller, A. Nenov, M. Olivucci, T. B. Pedersen, D. Peng, F. Plasser, B. Pritchard, M. Reiher, I. Rivalta, I. Schapiro, J. Segarra-Martí, M. Stenrup, D. G. Truhlar, L. Ungur, A. Valentini, S. Vancoillie, V. Veryazov, V. P. Vysotskiy, O. Weingart, F. Zapata, R. Lindh, *J. Comput. Chem.* **2016**, *37*, 506–541; b) L. F. Chibotaru, L. Ungur, *J. Chem. Phys.* **2012**, *137*, 064112.

Manuscript received: January 23, 2019

Revised manuscript received: February 19, 2019

Accepted manuscript online: February 20, 2019

Version of record online: March 27, 2019